Processing and Application of Ceramics 13 [3] (2019) 229–234
https://doi.org/10.2298/PAC1903229L

Preparation, characterization and formation mechanism of single-crystal zirconia micro-sheets

Jianmin Liu[1], Tao Wang[2], Weihui Jiang[1,2,*], Guo Feng[1], Lifeng Miao[1], Ting Chen[1], Qian Wu[1], Sanhai Wang[2]

[1]*National Engineering Research Center for Domestic and Building Ceramics, Jingdezhen, Jiangxi 333001, China*

[2]*School of Material Science and Engineering, Jingdezhen Ceramic Institute, Jingdezhen, Jiangxi 333403, China*

Received 23 January 2019; Received in revised form 22 May 2019; Accepted 10 July 2019

Abstract

Zirconia micro-sheets were prepared by molten salt method using the salt mixture of NaCl and NaF. FE-SEM, TEM, EDS, DTA-TG, XRD, Raman and FT-IR techniques were employed to characterize the morphology, phase composition and formation mechanism of the ZrO_2 micro-sheets. The obtained monoclinic ZrO_2 micro-sheets with exposed {100} facets show an average thickness of 0.2 μm. The growth of the ZrO_2 micro-sheets is proved to be assisted by the addition of fluoride. On the one hand, the addition of fluoride promotes the mass transfer of zirconia through the formation of zirconium fluoride complexes (ZrF_7^{3-}). On the other hand, fluoride adsorbed on the surface of zirconia stabilizes {100} facets and lead to the exposure of {100} facets in the final product.

Keywords: *zirconia micro-sheet, molten salt method, fluoride, crystal growth*

I. Introduction

As a typical structural and functional material, ZrO_2 has been extensively used in the field of ceramic tools, catalysts and catalyst supports, oxygen sensors, solid fuel cells and biomaterials owing to its excellent physical and chemical properties, such as high melting point, good chemical and mechanical stability, high toughness, ionic conductivity, excellent wear resistance and biocompatibility [1–4]. Recently, micro-sized single-crystal zirconia with significant recoverable shape deformation has received growing interest in the field of shape memory ceramics because of its fewer defects and high specific surface area for the relaxation of transformation mismatch stress [5,6]. In view of this, the as-prepared ZrO_2 micro-sheets in this work may be a good candidate for the shape memory ceramics. Up to now, a wide range of ZrO_2 morphologies such as rods [7], tetragonal stars [8], fibres [9], belts [10] and flowers [11] have been prepared by using hydrothermal method and template method. However, little effort has been reported to fabricate ZrO_2 micro-sheets. Since the facile ionic- liquid environment is favourable for the fast mass transfer [12], molten salt method has been preferentially employed to prepare the ZrO_2 micro-sheets in this work. Moreover, molten salt method has been proved to be a practical way for the preparation of Y_2O_3-stablized ZrO_2 [13], thus the further achievement of stabilized ZrO_2 micro-sheets can be better served as shape memory ceramics.

For typical molten salt synthesis, ZrO_2 micro-sheets were synthesized by the growth from salt mixtures of NaCl and NaF. The microstructure of the ZrO_2 micro-sheets was characterized and the formation mechanism was also discussed.

II. Experimental section

All the starting materials including $ZrOCl_2 \cdot 8\,H_2O$, NaCl and NaF were analytical reagents and used without further purification. The powders of 2 g $ZrOCl_2 \cdot 8\,H_2O$, 2 g NaCl and 0.2 g NaF (mass ratio 10 : 10 : 1) were mixed and ground for 15 min in an agate mortar, then the mixture was transported into a corun-

* Corresponding author: tel: +86 798 8499328,
e-mail: *whj@jci.edu.cn*

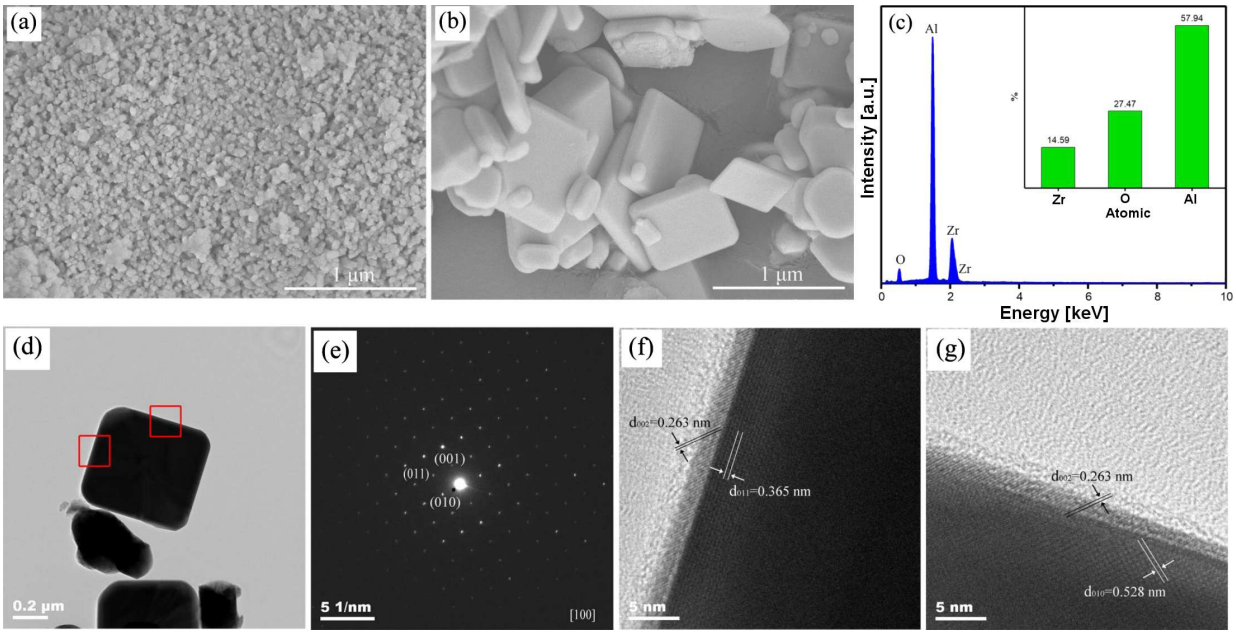

Figure 1. FE-SEM images of the samples grown from (a) NaCl, (b) NaCl/NaF, (c) EDS spectrum of the sample grown from NaCl/NaF, (d) TEM image, (e) SAED pattern, (f-g) HR-TEM images

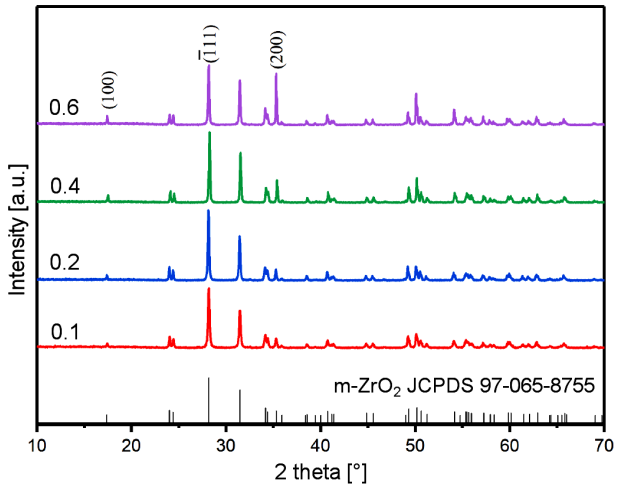

Figure 2. XRD patterns of the samples synthesized with different amount of NaF (g)

dum crucible with a lid and annealed at 800 °C for 5 h. After naturally cooling down to room temperature, the white powders were collected and washed three times with deionized water, followed by one washing with ethanol. Finally, the product was obtained by drying at 70 °C for 8 h.

The surface morphology and chemical composition of the as-prepared products were studied by FE-SEM (Hitachi SU8010) equipped with EDS. The DTA and TG analyses of the precursor mixture were performed on NETZSCH STA449C (heating rate 10 °C/min, air atmosphere). The microstructure of the ZrO_2 micro-sheets was characterized by TEM (JEOL JSM-2010). The phase composition of the as-prepared products was analysed by XRD (Bruker D8 advance) using Cu Kα radiation (λ = 0.154 nm). FT-IR spectrum was acquired on Nicolet 5700 infrared spectrometer. Raman spectra were obtained from Raman spectrometer (Renishaw in Via) with 532 nm incident photons from an Ar ion laser.

III. Results and discussion

FE-SEM images of the samples grown from NaCl and NaCl/NaF are shown in Figs. 1a and 1b, respectively. When NaF is introduced into the molten salt, the dramatic morphology changes from tiny particles to micro-sheets can be observed, suggesting that the addition of NaF plays an important role in the formation of the micro-sheets. The thickness of the obtained micro-sheets varies from 0.1 μm to 0.3 μm and the average thickness is about 0.2 μm. EDS analysis was performed on an aluminium foil and the EDS spectrum (Fig. 1c) has indicated that the sample is only composed of the element of Zr and O with a ratio of Zr to O approximately equal to 1 : 2, which is in agreement with the formula of ZrO_2. The typical TEM image (Fig. 1d) further confirms its sheet-shape structure with no distinct defects.

The legible SAED pattern (Fig. 1e) viewed from [100] zone axis indicates the single crystal nature of the micro-sheets and the three spots are indexed as (001), (010) and (011) facets of monoclinic zirconia (m-ZrO_2, JCPDS 97-065-8755). The lattice fringes (Fig. 1f and Fig. 1g) with an interplanar lattice spacing of 0.365 nm, 0.528 nm and 0.263 nm correspond to (011), (010) and (002) atomic planes, respectively. In addition, Fig. 2 shows the XRD patterns of the sample synthesized with different amount of NaF. All of the diffraction peaks of the samples can be indexed as monoclinic zirconia (m-ZrO_2). It can be seen that the peak intensity of (100) and parallel (200) atomic planes become stronger with the increase of NaF, whereas the peak intensity of ($\bar{1}$11) facet is reduced when the amount of NaF is be-

Table 1. Variation of diffraction peak intensity with the increase of NaF

Amount of NaF [g]	Peak intensity			Peak intensity ratio	
	$I_{\bar{1}11}$	I_{100}	I_{200}	$I_{100}/I_{\bar{1}11}$	$I_{200}/I_{\bar{1}11}$
0.1	757	62	121	0.082	0.160
0.2	890	75	145	0.084	0.162
0.4	889	98	288	0.110	0.324
0.6	754	118	646	0.156	0.414

yond 0.4 g. To intuitively understand the peak intensity changes, Table 1 gives the variation of diffraction peak intensity with the increase of NaF. The peak intensity ratios of $I_{100}/I_{\bar{1}11}$ and $I_{200}/I_{\bar{1}11}$ get promoted with the increase of NaF addition, which indicates that more (100) facets are exposed with the increase of NaF. This phenomenon also suggests that the growth habit of ZrO_2 is greatly affected by the NaF. On the basis of above results, it can be confirmed that {100} facets are exposed on the bottom and top surfaces of the micro-sheets.

DTA-TG curves of the precursor mixture with the addition of NaF are shown in Fig. 3. There are two obvious weight loss stages at 30–500 °C and 700–1100 °C in TG curve. The first weight loss is about 26.36%, corresponding to the evaporation of H_2O and HCl produced by the decomposition of $ZrOCl_2 \cdot 8\,H_2O$ [14]. The second weight loss is about 54.21%, which is attributed to the volatilization of the molten salt. In DTA curve, two adjacent endothermic peaks centred at 83 and 147 °C are caused by the different dehydration stages of $ZrOCl_2 \cdot 8\,H_2O$ [15]. The distinct endothermic peak at 753 °C is assigned to the melting of salt mixture, paralleling with little weight loss in TG curve. The broad endothermic peak ranging from 874 to 945 °C can be attributed to the volatilization of the molten salt. Thus, a completely melted ionic-liquid environment can be achieved at 800 °C based on above analysis, which is greatly beneficial to the mass transfer and the crystal growth of ZrO_2.

XRD patterns of the samples synthesized with or without NaF are shown in Fig. 4. The sample synthesized with the addition of NaF shows enhanced peak intensity of monoclinic zirconia (m-ZrO_2) and no secondary phase such as tetragonal zirconia (t-ZrO_2) is observed. However, the sample synthesized without NaF shows diffraction peaks of t-ZrO_2. The t-ZrO_2 is produced by the decomposition of $ZrOCl_2 \cdot 8\,H_2O$ and exists in metastable forms due to the small size effect for which the critical size is about 28 ± 6 nm [16]. The Scherrer equation $d = K \cdot \lambda/(\beta \cos\theta)$ [17] was applied to calculate the average crystallite size d (θ is the diffraction angle, K is 0.89, λ is X-ray wavelength, β is the full width at half maximum). The average crystallite sizes of t-ZrO_2 and m-ZrO_2 are estimated to be 32 and 44 nm, respectively, where the average crystallite size of t-ZrO_2 satisfies the small size effect, explaining the existence of metastable t-ZrO_2 at room temperature. These XRD results reveal that the addition of NaF can effectively promote the crystal growth and crystallinity of the obtained ZrO_2, which has also been confirmed by the FE-SEM images.

Raman spectra of the samples synthesized with or without NaF are shown in Fig. 5. The Raman spectra of

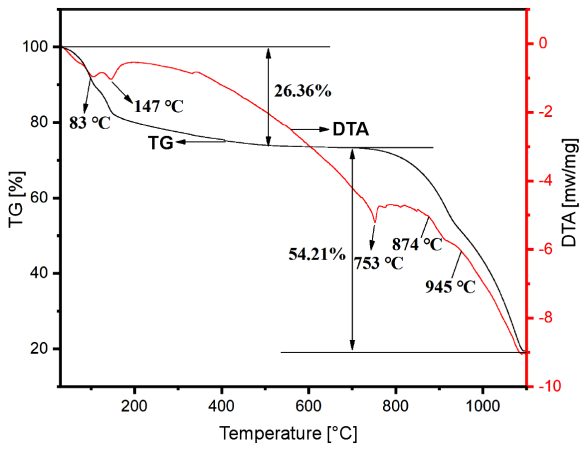

Figure 3. DTA-TG curves of the precursor mixture with the addition of NaF

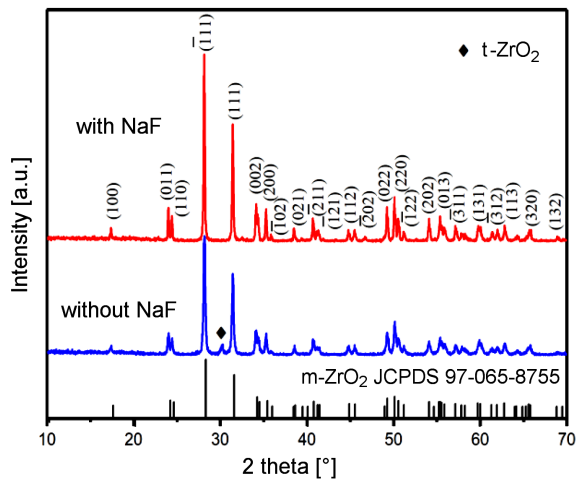

Figure 4. XRD patterns of the samples synthesized with or without NaF

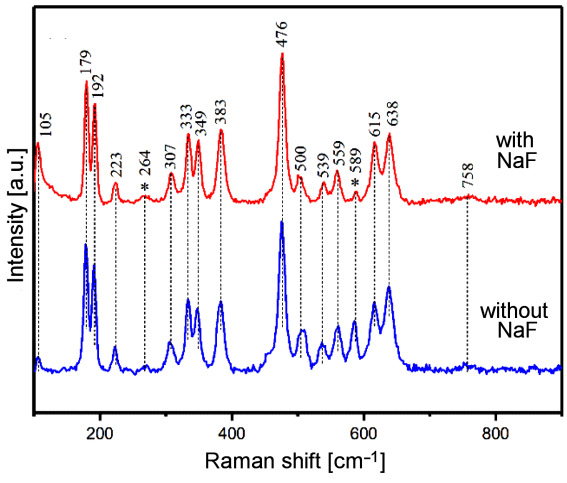

Figure 5. Raman spectra of the samples synthesized with or without NaF

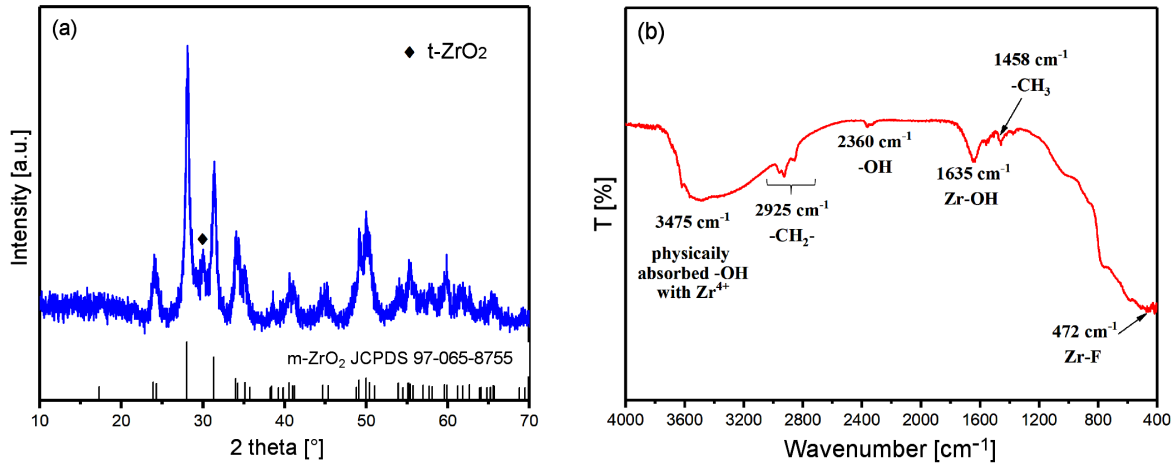

Figure 6. XRD pattern (a) and FT-IR spectrum (b) of the sample synthesized at 300 °C

both samples are almost the same in spite of the different peak intensities of Raman bands at 589 cm^{-1} marked as asterisks (*). Among 17 Raman bands observed in both samples, except two peaks at 264 and 589 cm^{-1} ascribed to t-ZrO_2 [18], all other bands are assigned to vibration modes of m-ZrO_2 [19]. Noticeably, the sample synthesized without NaF shows a relatively stronger peak intensity at 589 cm^{-1} than the sample synthesized with NaF, indicating the higher content of t-ZrO_2 in the former, which is consistent with the XRD results. The existence of t-ZrO_2 in micro-sheets detected by Raman unlike with XRD confirms again that Raman spectrum is a very useful technique for the determination of crystal phase of zirconia. In the ionic-liquid salt system, it has been proved that the addition of the fluoride can effectively promote the mass transfer process of ZrO_2, which is achieved by the formation of chemical species ZrF_7^{3-} as shown in following equation [20,21]:

$$ZrO_2 + 7\,F^- \longrightarrow ZrF_7^{3-} + 2\,O^{2-} \qquad (1)$$

Thus, the crystal size of the obtained ZrO_2 can rapidly grow from nanoscale to microscale. In addition, due to the small amount of fluoride in this work, ZrF_7^{3-} species remain dissolved in the melt without forming other compounds [20], which is also confirmed by the XRD and Raman analysis.

Since the early growth stage of the ZrO_2 below melting temperature is crucial to further understand the formation mechanism of sheet-shaped ZrO_2, the XRD pattern and FT-IR spectrum of the sample synthesized at 300 °C for 5 h are given in Fig. 6. As shown in Fig. 6a, the pattern is mainly indexed as m-ZrO_2 except for some diffraction peaks belonging to t-ZrO_2. In addition, the broad diffraction peaks indicate the small size and low crystallinity of obtained m-ZrO_2, which is favourable for the growth of ZrO_2 micro-sheets relative to the highly crystalline ZrO_2 [12]. Fig. 6b shows the FT-IR spectrum of the sample synthesized at 300 °C. The broad peak around 3475 cm^{-1} is attributed to the physically absorbed −OH with Zr^{4+}. Bands at 2800–2980 cm^{-1} and 1460 cm^{-1} are assigned to the $-CH_2-$ stretching vibration and $-CH_3$ band vibration [22], respectively, which arise from the residual ethanol in the sample. The peak centred at 2360 cm^{-1} is due to the stretching and bending vibrations of −OH groups, while the band at 1635 cm^{-1} is associated with the bending vibrations of Zr−OH [23]. Accordingly, the weak peak at 472 cm^{-1} is assigned to the band of Zr−F, suggesting that the ZrO_2 shows high affinity for F^- [24]. A growth mechanism for ZrO_2 micro-sheets can be proposed based on the above analysis. As shown in Fig. 7, tiny m-ZrO_2 is formed at the initial growth stage and its theoretical equilibrium shape is composed of four

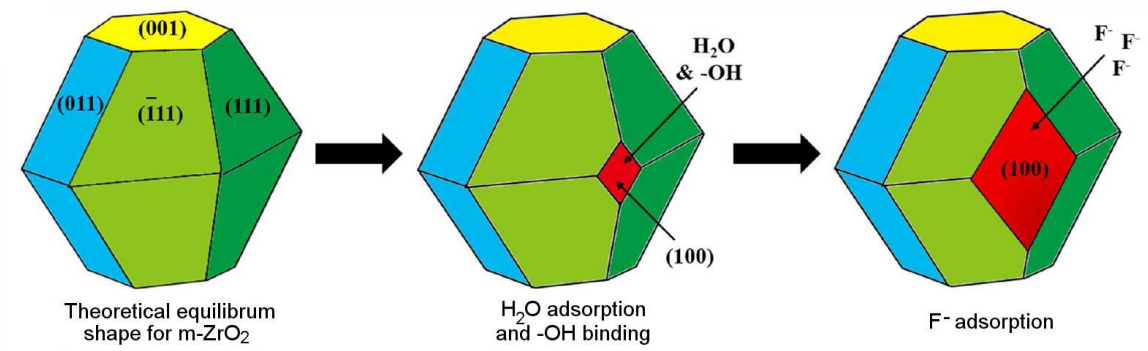

Figure 7. Schematic drawings for the formation of ZrO_2 micro-sheet

($\bar{1}11$), (111), (011), and (001) facets. The surface energies of these facets increase in the following order: ($\bar{1}11$) < (111) < (011) < (001) [25]. In addition, the facet with higher energy means faster growth rate in the crystal growth. Then, the adsorbed H_2O and banded −OH on the surface of ZrO_2 give a chance for the appearance of new (100) facet [25]. It should be noticed that (100) facet possesses higher surface energy than the former four facets [25,26]. So, (100) facets show stronger adsorption for F^- than other four facets. Correspondingly, the F^- adsorption leads to the inverse surface energy, of which the (100) facet is the lowest one. This similar phenomenon is also observed in the stabilization of highly reactive {001} facets in TiO_2 by the addition of fluoride [27]. Finally, the sheet-shaped ZrO_2 with exposed {100} facets is achieved via the further growth of ZrO_2 in the liquid salt flux.

IV. Conclusions

This work has developed a facile molten salt method to fabricate ZrO_2 micro-sheets. The as-prepared ZrO_2 micro-sheets with average thickness of 0.2 μm show exposed {100} facets and are characterized with the monoclinic structure. The addition of NaF, essential for the preparation of ZrO_2 micro-sheets, is found to play an important role in accelerating the mass transfer of ZrO_2 through the formation of ZrF_7^{3-} and controlling the sheet-shape by the F^- adsorption on the surface of ZrO_2. Moreover, the special micro-sized single-crystal ZrO_2 sheets will find application in the shape memory ceramics in the future.

Acknowledgement: The authors are thankful to the Fund for National Natural Science Foundation of China (51662016), the Fund for Distinguished Young Scholars of Jiangxi Province (20171BCB23071), the Fund for Science Foundation of Jiangxi Province (GJJ160881).

References

1. C.L. Jiang, F. Wang, N.Q. Wu, X. Liu, "Up- and down-conversion cubic zirconia and hafnia nanobelts", *Adv. Mater.*, **20** [24] (2008) 4826–4829.
2. J. Chevalier, "What future for zirconia as a biomaterial?", *Biomaterials*, **27** (2006) 535–543.
3. G. Feng, W.H. Jiang, J.M. Liu, Q. Zhang, Q. Wu, L. Miao, "A novel green nonaqueous sol-gel process for preparation of partially stabilized zirconia nanopowder", *Process. Appl. Ceram.*, **11** [3] (2017) 220–224.
4. H.Q. Cao, X.Q. Qiu, B. Luo, Y. Liang, Y.H. Zhang, R.Q. Tan, M.J. Zhao, Q.M. Zhu, "Synthesis and room-temperature ultraviolet photoluminescence properties of zirconia nanowires", *Adv. Funct. Mater.*, **14** [3] (2004) 243–246.
5. A. Lai, Z. Du, C.L. Gan, C.A. Schuh, "Shape memory and superelastic ceramics at small scales", *Science*, **341** [6153] (2013) 1505–1508.
6. X.M. Zeng, Z. Du, N. Tamura, Q. Liu, C.A. Schuh, C.L. Gan, "In-situ studies on martensitic transformation and high-temperature shape memory in small volume zirconia", *Acta Mater.*, **134** [1] (2017) 257–266.
7. L. Kumari, W.Z. Li, J.M. Xu, R.M. Leblanc, D.Z. Wang, Y. Li, H. Guo, J. Zhang, "Controlled hydrothermal synthesis of zirconium oxide nanostructures and their optical properties", *Cryst. Growth Des.*, **9** [9] (2009) 3874–3880.
8. Z.X. Shu, X.L. Jiao, D.R. Chen, "Hydrothermal synthesis and selective photocatalytic properties of tetragonal starlike ZrO_2 nanostructures", *Cryst. Eng. Comm.*, **15** [21] (2013) 4288–4294.
9. E. Formo, P.H.C. Camargo, B. Lim, M. Jiang, Y. Xia, "Functionalization of ZrO_2 nanofibers with Pt nanostructures: The effect of surface roughness on nucleation mechanism and morphology control", *Chem. Phys. Lett.*, **476** (2009) 56–61.
10. Q.X. Gao, X.F. Wang, X.C. Wu, Y.R. Tao, J.J. Zhu, "Mesoporous zirconia nanobelts: preparation, characterization and applications in catalytical methane combustion", *Micropor. Mesopor. Mater.*, **143** [2] (2011) 333–340.
11. G. Poungchan, B. Ksapabutr, M. Panapoy, "One-step synthesis of flower-like carbon-doped ZrO_2 for visible-light-responsive photocatalyst", *Mater. Des.*, **89** (2016) 137–145.
12. M.A. Einarsrud, T. Grande, "1D oxide nanostructures from chemical solutions", *Chem. Soc. Rev.*, **43** [7] (2014) 2187–2199.
13. D. Hamon, M. Vrinat, M. Breysse, B. Durand, M. Jebrouni, M. Roubin, P. Magnoux, T. des Courières, "Molten salt preparation of stabilized zirconia catalysts: characterization and catalytic properties", *Catal. Today*, **10** [4] (1991) 613–627.
14. N. Gorodylova, P. Šulcová, M. Bosacka, E. Filipek, "DTA-TG and XRD study on the reaction between $ZrOCl_2 \cdot 8\,H_2O$ and $(NH_4)_2HPO_4$ for synthesis of ZrP_2O_7", *J. Therm. Anal. Calorim.*, **118** [2] (2014) 1095–1100.
15. J. Scholz, S. Kerstin, A.J. Mcquillan, "In situ infrared spectroscopic analysis of the water modes of $[Zr_4(OH)_8(H_2O)_{16}]_8^+$ during the thermal dehydration of $ZrOCl_2 \cdot 8\,H_2O$", *J. Phys. Chem. A*, **114** [29] (2010) 7733–7741.
16. A.V. Radha, O. Bomati-Miguel, S.V. Ushakov, A. Navrotsky, P. Tartaj, "Surface enthalpy, enthalpy of water adsorption, and phase stability in nanocrystalline monoclinic zirconia", *J. Am. Ceram. Soc.*, **92** [1] (2009) 133–140.
17. G. Xu, Y.W. Zhang, C.S. Liao, C.H. Yan, "Doping and grain size effects in nanocrystalline ZrO_2-Sc_2O_3 system with complex phase transitions: XRD and Raman studies", *Phys. Chem. Chem. Phys.*, **6** [23] (2004) 5410–5418.
18. A.P. Mirgorodsky, M.B. Smirnov, P.E. Quintard, "Phonon spectra evolution and soft-mode instabilities of zirconia during the c-t-m transformation", *J. Phys. Chem. Solids*, **60** [7] (1999) 985–992.
19. P.E. Quintard, P. Barbéris, A.P. Mirgorodsky, T. Merle-Méjean, "Comparative lattice-dynamical study of the Raman spectra of monoclinic and tetragonal phases of zirconia and hafnia", *J. Am. Ceram. Soc.*, **85** (2002) 1745–1749.
20. P. Afanasiev, C. Geantet, "Synthesis of solid materials in molten nitrates", *Coord. Chem. Rev.*, **178-180** (1998) 1725–1752.
21. P. Afanasiev, "Synthesis of dispersed ZrO_2 in the fluoride-doped molten $NaNO_3$-KNO_3 mixtures", *J. Mater. Sci. Lett.*, **16** (1997) 1691–1692.

22. T. Chen, X.J. Zhang, W.H. Jiang, J. Liu, W. Jiang, Z. Xie, "Synthesis and application of C@$ZrSiO_4$ inclusion ceramic pigment from cotton cellulose as a colorant", *J. Eur. Ceram. Soc.*, **36** [7] (2016) 1811–1820.
23. D. Sarkar, D. Mohapatra, S. Ray, S. Bhattacharyya, S. Adak, N. Mitra, "Nanostructured Al_2O_3-ZrO_2 composite synthesized by sol-gel technique: powder processing and microstructure", *J. Mater. Sci.*, **42** [5] (2007) 1847–1855.
24. J. Wang, X. Lin, X. Luo, Y. Long, "A sorbent of carboxymethyl cellulose loaded with zirconium for the removal of fluoride from aqueous solution", *Chem. Eng. J.*, **252** (2014) 415–422.
25. W. Piskorz, J. Gryboś, F. Zasada, S. Cristol, J.F. Paul, A. Adamski, Z. Sojka, "Periodic DFT and atomistic thermodynamic modeling of the surface hydration equilibria and morphology of monoclinic ZrO_2 nanocrystals", *J. Phys. Chem. C*, **115** [49] (2011) 24274–24286.
26. A. Christensen, E.A. Carter, "First-principles study of the surfaces of zirconia", *Phys. Rev. B*, **58** [12] (1998) 8050–8064.
27. H.G. Yang, C.H. Sun, S.Z. Qiao, J. Zou, G. Liu, S.C. Smith, H.M. Cheng, G.Q. Lu, "Anatase TiO_2 single crystals with a large percentage of reactive facets", *Nature*, **453** [7195] (2008) 638–641.